Biology of Reproduction, 2023, **109(2)**, 192–203
https://doi.org/10.1093/biolre/ioad064
Advance access publication date 9 June 2023
Research Article

Mitochondrial uncouplers impair human sperm motility without altering ATP content†

Will M. Skinner[1,2], Natalie T. Petersen[2,3], Bret Unger[4], Shaogeng Tang[5,6], Emiliano Tabarsi[2,7], Julianna Lamm[2,8], Liza Jalalian[9], James Smith[10], Ambre M. Bertholet[11,12], Ke Xu[4,13,14], Yuriy Kirichok[11] and Polina V. Lishko[1,2,15,*]

[1]Endocrinology Graduate Group, University of California, Berkeley, Berkeley, California, USA
[2]Department of Molecular and Cell Biology, University of California, Berkeley, Berkeley, California, USA
[3]Department of Obstetrics and Gynecology, Stanford University School of Medicine, Palo Alto, California, USA
[4]Department of Chemistry, University of California, Berkeley, Berkeley, California, USA
[5]Department of Biochemistry, Stanford University School of Medicine, Stanford, California, USA
[6]Sarafan ChEM-H, Stanford University, Stanford, California, USA
[7]Keck School of Medicine, University of Southern California, Los Angeles, California, USA
[8]Dewpoint Therapeutics, Boston, Massachusetts, USA
[9]Department of Obstetrics and Gynecology, University of California, San Francisco Center for Reproductive Health, San Francisco, California, USA
[10]Department of Urology, University of California, San Francisco, San Francisco, California, USA
[11]Department of Physiology, University of California, San Francisco, San Francisco, California, USA
[12]Department of Physiology, David Geffen School of Medicine, University of California, Los Angeles, Los Angeles, California, USA
[13]California Institute for Quantitative Biosciences, University of California, Berkeley, California, USA
[14]Chan Zuckerberg Biohub, San Francisco, California, USA
[15]Department of Cell Biology & Physiology, Washington University School of Medicine in St. Louis, St. Louis, Missouri, USA

***Correspondence:** Department of Cell Biology and Physiology, Washington University in St. Louis School of Medicine, St. Louis, MO 63110, USA. Tel: 314-362-3566; E-mail: lishko@wustl.edu

†**Grant Support:** This work was furthered by the support and guidance of Dr. Denise Schichnes, using the equipment of the CNR Biological Imaging Facility at the University of California, Berkeley. Research reported in this publication was supported in part by the National Institutes of Health S10 program under award number 1S10OD018136-01. The content is solely the responsibility of the authors and does not necessarily represent the official views of the National Institute of Health. The authors also wish to thank Dr. Liliya Gabelev Khasin, Dr. Caroline Williams, Dr. Lisa Treidel, and Dr. Erwin Goldberg for their assistance with this project. This work was supported by an Irving H. Wiesenfeld Fellowship administered by the UC Berkeley Center for Emerging and Neglected Diseases to WMS, a Male Contraceptive Initiative Graduate Fellowship to PVL, and Liliya Gabelev Khasin, NIH NICHD (grant K99HD104924 to ST), NIGMS (grant R35GM136415 to YK), Pew Biomedical Scholars Award to PVL and KX and Bakar Fellow Spark Award to PVL. This material is based upon work supported by the National Science Foundation Graduate Research Fellowship Program (under grant numbers DGE 1752814 and DGE 2146752 to WMS). Any opinions, findings, and conclusions or recommendations expressed in this material are those of the author(s) and do not necessarily reflect the views of the National Science Foundation.

Abstract

In human spermatozoa, the electrochemical potentials across the mitochondrial and plasma membranes are related to sperm functionality and fertility, but the exact role of each potential has yet to be clarified. Impairing sperm mitochondrial function has been considered as an approach to creating male or unisex contraceptives, but it has yet to be shown whether this approach would ultimately block the ability of sperm to reach or fertilize an egg. To investigate whether the mitochondrial and plasma membrane potentials are necessary for sperm fertility, human sperm were treated with two small-molecule mitochondrial uncouplers (niclosamide ethanolamine and BAM15) that depolarize membranes by inducing passive proton flow, and evaluated the effects on a variety of sperm physiological processes. BAM15 specifically uncoupled human sperm mitochondria while niclosamide ethanolamine induced proton current in the plasma membrane in addition to depolarizing the mitochondria. In addition, both compounds significantly decreased sperm progressive motility with niclosamide ethanolamine having a more robust effect. However, these uncouplers did not reduce sperm adenosine triphosphate (ATP) content or impair other physiological processes, suggesting that human sperm can rely on glycolysis for ATP production if mitochondria are impaired. Thus, systemically delivered contraceptives that target sperm mitochondria to reduce their ATP production would likely need to be paired with sperm-specific glycolysis inhibitors. However, since niclosamide ethanolamine impairs sperm motility through an ATP-independent mechanism, and niclosamide is FDA approved and not absorbed through mucosal membranes, it could be a useful ingredient in on-demand, vaginally applied contraceptives.

Summary Statement: Here we find that human sperm can maintain their ATP levels without mitochondrial oxidative phosphorylation, and we improve the subcellular localization of Adenosine Nucleotide Translocator 4; these findings will help focus future development of sperm-targeted contraceptives.

Keywords: sperm metabolism, mitochondrial uncouplers, sperm motility, contraception.

Received: November 15, 2022. **Revised:** April 22, 2023. **Accepted:** June 1, 2023.

Introduction

Human sperm are vigorously motile cells that require a well-regulated electrochemical potential across both the plasma membrane [1–3] and the mitochondrial membrane [4–7]. However, much is still unknown about the physiological importance of each of these potentials since it has been difficult to disentangle their roles.

Small molecule uncouplers are a class of compounds that depolarize electrochemically charged membranes by passively shuttling protons down their concentration gradient. The name comes from the fact that they are able to "uncouple" the mitochondrial electron transport chain from the adenosine triphosphate (ATP) synthase machinery, thus causing cells to consume more oxygen and chemical energy substrates while producing less ATP [8]. These uncouplers were previously assumed to non-specifically pass through any phospholipid bilayer [9], but in 2014, Kenwood et al. [10] developed BAM15, an uncoupler that specifically depolarizes the mitochondrial membrane potential without affecting the plasma membrane, and in 2022 Bertholet et al. [11] showed that BAM15 and several other uncouplers actually perform a majority of their uncoupling activity through binding with the adenine nucleotide translocase (ANT) family of proteins.

The fourth isoform of the ANT family (ANT4) is specifically expressed in gametes [12, 13], and required for spermatogenesis [14], but has an unclear role in mature sperm cells. Since its discovery, ANT4 has been seen as an attractive candidate for the development of a male contraceptive [14–17], and efforts have been made to develop specific ANT4 inhibitors [16, 17]. These inhibitors would theoretically block sperm mitochondrial ATP production, but no one has yet proved that human sperm cells would be unable to function without mitochondrially produced ATP. In fact, there has been persistent debate about the role of mitochondrial oxidative phosphorylation in sperm physiology, with metabolic studies showing that glycolysis is sufficient for human sperm ATP production [18], but physiological and clinical studies showing that proper mitochondrial functionality is correlated with high fertility in humans [5, 6, 19, 20].

Therefore, in this work, we utilized a pair of small molecule uncouplers with different levels of mitochondrial specificity to investigate the physiological importance of the mitochondrial membrane potential (which is required for mitochondrial ATP production) and the plasma membrane potential to various human sperm functions necessary for fertilization, including motility, hyperactivation, and the acrosome reaction.

Results

NEN and BAM15 both decrease human sperm mitochondrial membrane potential, but only NEN induces H^+ current across the plasma membrane

After a preliminary screening process, two small molecule uncouplers were chosen as representative uncouplers: BAM15 (N5,N6-*bis*(2-fluorophenyl)-[1,2,5]oxadiazolo[3,4-*b*]pyrazine-5,6-diamine) and niclosamide ethanolamine (NEN) (Figure 1A). These two compounds were chosen because, in somatic cell types, BAM15 is known to be a protein-mediated [11], mitochondrial-specific [10, 21] uncoupler, and niclosamide is known to uncouple both mitochondria [8, 22] and late endosomes [23]. Figure 1B shows a schematic of both protein-mediated mitochondrial uncoupling and protein-independent membrane uncoupling. Given the uniqueness of sperm and their mitochondria, we began by confirming that the two compounds work as expected in human sperm.

Live human sperm cells were treated with varying concentrations of each compound for 30 min at 37°C in non-capacitating media at pH 7.4, after which cells were stained with MitoTracker Red CMX-Ros and mitochondrial membrane potential (MMP) was qualitatively assessed using flow cytometry (Figure 1C and D, Supplementary Figure S1A–C) and fluorescence microscopy (Figure 1E). BAM15 and NEN were both able to dose-dependently reduce midpiece fluorescence and therefore MMP, with IC_{50} values below 10 μM (Figure 1C). The DMSO vehicle with which compounds were delivered did not have a dose-dependent effect on mitochondrial fluorescence (Supplementary Figure S1D) and none of the compounds decreased sperm viability as measured by propidium iodide permeability (Supplementary Figure S1E) in either non-capacitated (Supplementary Figure S1F) or capacitated (Supplementary Figure S1G) sperm.

To assess whether these two uncouplers were in fact acting through different mechanisms in human sperm, the effects of each compound on sperm plasma membrane H^+-ion current were measured using whole-cell patch-clamp electrophysiology. In this assay, 10 μM NEN induced a significant inward transmembrane H^+-ion current at negative voltages while 10 μM BAM15 had no effect (Figure 1F, G). The DMSO vehicle also induced no discernable H^+ current (Figure 1F, Supplementary Figure S1H).

NEN-induced mitochondrial H^+ current is partially protein mediated but more non-specific than BAM15-induced current

In somatic, non-thermogenic tissues of the body, ANT proteins are known to mediate mild mitochondrial uncoupling under physiological conditions and in the presence of exogenous uncouplers by allowing H^+ influx across the inner mitochondrial membrane [11, 24]. Around 80% of BAM15's uncoupling effect has been shown to be mediated by these ANT proteins [11]. Therefore, we investigated whether NEN-induced uncoupling is also mediated by the ANT family of proteins. To do this, we performed mitochondrial patch-clamp electrophysiology, through which it is possible to directly measure current across the inner mitochondrial membrane (Figure 1H). Indeed, in mouse heart mitochondria, which abundantly express ANT1 [25], 500 nM NEN induced a strong inward H^+ current at physiological pH and negative voltage (Figure 1I). This H^+ current was reduced by approximately 25% in the presence of 1 μM carboxyatractyloside (CATR), a known ANT inhibitor, and by approximately 40% in heart mitochondria from ANT1-knockout mice (Figure 1I, J). This indicates that the NEN-induced current is partially mediated by ANT proteins, but that its activity is relatively more non-specific than BAM15's.

ANT4 is localized to the human sperm mitochondria

Given that NEN induces robust plasma membrane H^+ current in human sperm (Figure 1F, G), that part of NEN's uncoupling in mitochondria is mediated by ANT proteins (Figure 1I, J), and that the sperm-specific ANT4 protein has been reported to be present in the sperm flagellum [26], it

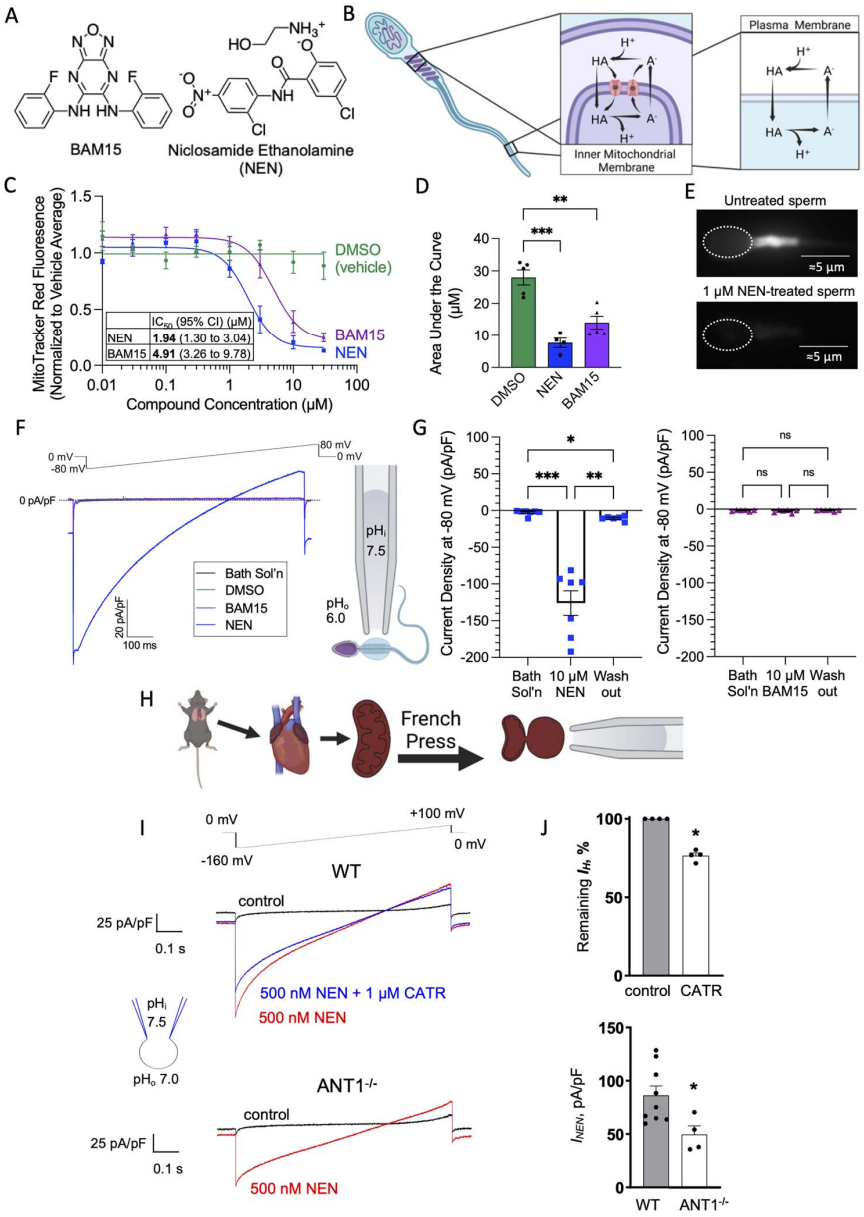

Figure 1. BAM15 specifically uncouples human sperm mitochondria, while NEN uncouples both sperm mitochondria and plasma membrane. (A) Chemical structures of BAM15 and NEN. (B) Model showing the possible mechanisms of action of small molecule uncouplers in the sperm mitochondria and plasma membrane, with both protein-mediated and membrane-mediated uncoupling occurring across the inner mitochondrial membrane, and only membrane-mediated uncoupling occurring across the plasma membrane. HA represents the protonated form of a small molecule uncoupler, A^- represents the deprotonated form, and H^+ represents free protons. (C) Effects of NEN and BAM15 on human sperm mitochondrial potential as measured by MitoTracker Red fluorescence, normalized to average fluorescence of the DMSO vehicle. Non-linear least-squares regression was performed on NEN and BAM15 using an unweighted [inhibitor] vs. response four-parameter model. DMSO data fitted to a horizonal line, based on the results of a regression model comparison using the extra sum-of-squares *F* test. (D) AUC analysis for data in (C). Error bars represent SEM, and each data point represents the area under the curve for all concentrations of one biological replicate, calculated directly from raw data points, not the non-linear regression line. Statistical significance was calculated using Dunnett's multiple comparisons test. (E) Representative fluorescence micrographs of sperm cells treated with MitoTracker Red CMX-Ros. (F) *Left*, representative electrophysiological traces showing the effect of vehicle and uncouplers on human sperm membrane H^+ current density. *Right*, diagram of sperm electrophysiology setup. Cytoplasmic droplet is magnified for visibility. (G) Quantification of maximal current densities in the presence of 10 μM NEN (left) and BAM15 (right) at a voltage of −80 mV. Error bars represent SEM, and significance calculated using Tukey's multiple comparisons test. (H) Diagram of mouse heart mitoplast isolation and preparation for whole-organelle inner membrane electrophysiology. (I) Representative whole-organelle electrophysiological traces of H^+ current density in response to voltage ramp protocols performed on mouse heart mitoplasts. Top, wild type; bottom, ANT1 knockout. (J) *Top*, quantification of NEN-induced H^+ current across mitochondrial inner membrane before and after application of 1 μM CATR, a known ANT inhibitor. *Bottom*, quantification of H^+ current density induced by 500 nM NEN in wild-type and ANT1-knockout mouse heart mitoplasts. Significances calculated by Student's unpaired *t*-test.

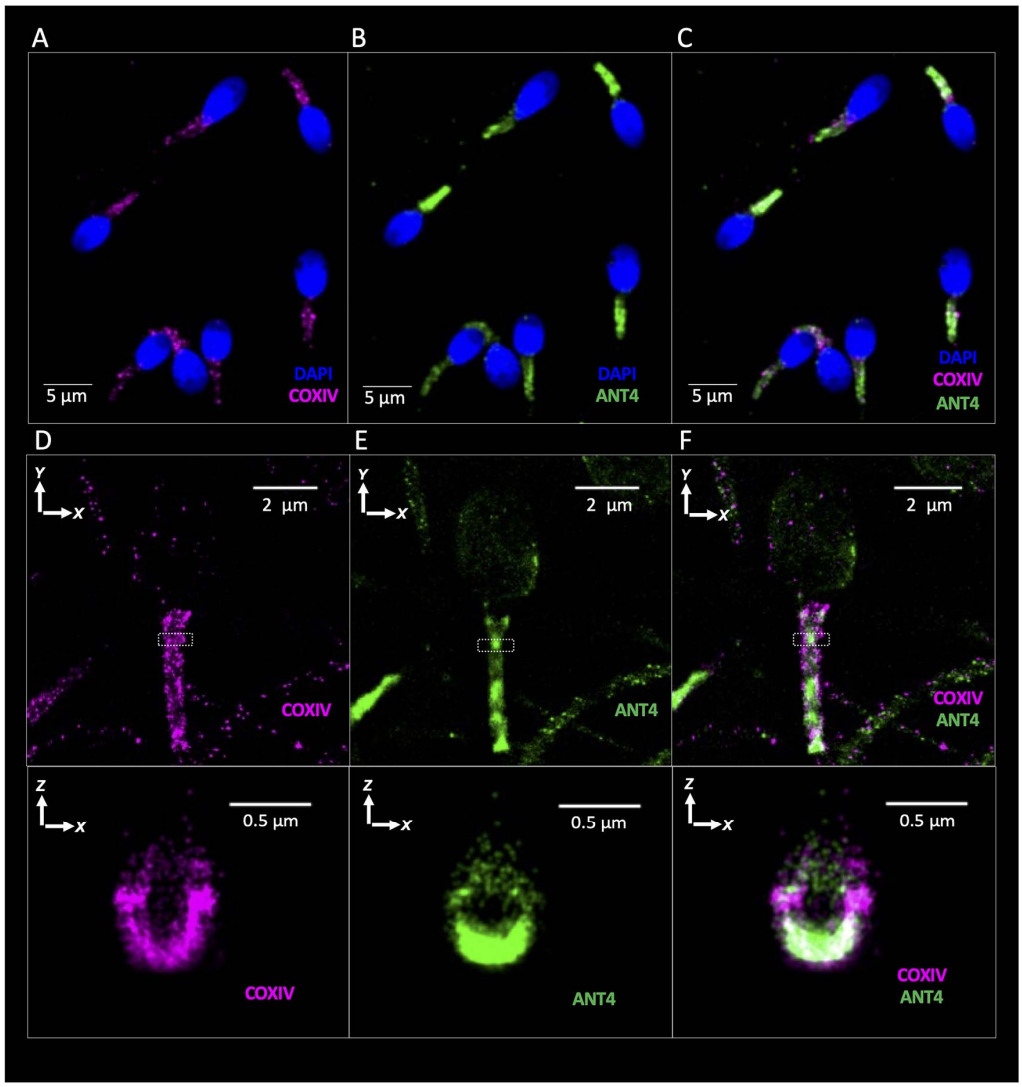

Figure 2. ANT4 is located in the human sperm mitochondria. (A–C) Confocal microscopy of human sperm immunocytochemistry showing localization of COXIV (magenta), ANT4 (green), and DAPI (blue). (D–F) STORM super-resolution microscopy of human sperm cells showing localization of COXIV (magenta) and ANT4 (green). Top panels: overhead view of sperm cells. Bottom panels: transverse plane of midpiece area indicated in top panels by white dotted box.

was necessary to confirm ANT4's cellular localization to see if any of NEN's observed plasma membrane current might be ANT mediated. Using a rabbit polyclonal antibody specific for human ANT4, which was validated both by the manufacturer and in-house (Supplementary Figure S2A–D), non-permeabilized human sperm cells showed no ANT4 signal (Supplementary Figure S2E), suggesting that ANT4 is not embedded in the plasma membrane. In permeabilized sperm cells, when excess primary antibody is used, some ANT4 staining is seen throughout the flagellum (Supplementary Figure S2F), but when primary antibody concentration is titrated down to an optimal concentration, ANT4 staining is restricted to the midpiece in a similar distribution to that of the inner mitochondrial membrane protein cytochrome *c* oxidase (COXIV) (Figure 2A–C). This finding was confirmed using stochastic optical reconstruction microscopy (STORM) on human sperm cells similarly costained for COXIV and ANT4 (Figure 2D–F, top). Upon virtual cross-sectioning of the midpiece, distributions of these two proteins formed rings of similar diameter and thickness (Figure 2D–F, bottom), consistent with mitochondrial localization. Together, these data suggest that NEN is acting as a non-specific protonophore in the human sperm plasma membrane. They also validate the use of these two compounds to investigate the differential physiological effects of impairing only mitochondrial membrane potential (BAM15) or both mitochondrial and plasma membrane potential (NEN).

NEN and BAM15 both impair human sperm basal motility

To begin exploring the physiological impacts of uncouplers on human sperm physiology, the effects of NEN and BAM15

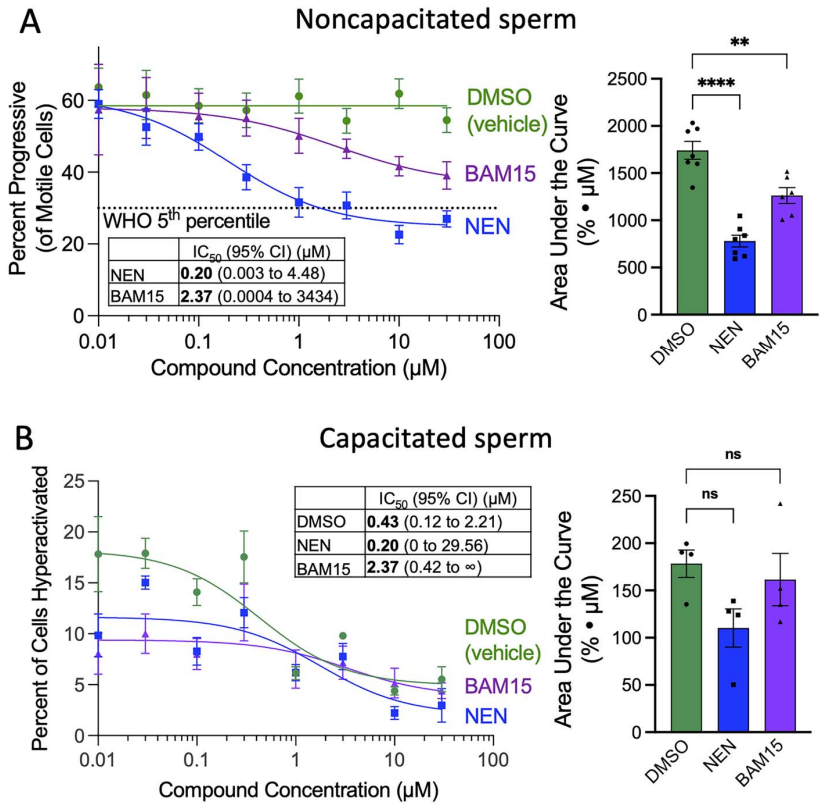

Figure 3. Effects of NEN and BAM15 on human sperm motility and hyperactivity as measured by computer-aided sperm analysis. (A) *Left*, effects of NEN and BAM15 on the percentage of human sperm showing progressive motility. At least 500 sperm cells were measured in each data point. Four-parameter non-linear least squares regression was performed, weighted by $1/Y^2$. Horizontal line fitted to DMSO data based on the results of a regression model comparison using the extra sum-of-squares *F* test. *Right*, AUC quantification for the graph at left. (B) *Left*, effects of compounds on the percentage of human sperm cells displaying hyperactivated motility. Three-parameter non-linear least squares regression performed, weighted by $1/Y^2$. At least 200 sperm cells were measured in each data point. To simplify the graph, the amount of DMSO vehicle is shown as the concentration of compound that would have been delivered by that amount of DMSO. Based on dilution procedures, the IC_{50} shown corresponds to an actual DMSO concentration of 0.0043%. *Right*, AUC quantification for the graph at left. Error bars in all plots represent SEM. In both (A) and (B), AUC was calculated directly from data points, not from non-linear regression lines, and each data point represents the area under the curve for all concentrations of one biological replicate. Statistical significance in AUC analyses was calculated using Dunnett's multiple comparisons test, and units in all AUC plots are the products of the *x* and *y* units in the relevant dose–response plot.

on sperm motility were observed using computer-aided sperm analysis (CASA). Thirty minutes of incubation with either NEN or BAM15 reduced the percent of non-capacitated sperm showing progressive motility (Figure 3A) and incubation with NEN reduced the average curvilinear velocity (Supplementary Figure S3A); NEN reduced sperm progressive motility percent below the 5th percentile of fertile men [27] and showed a sub-micromolar IC_{50} (Figure 3A).

The effect of compounds on sperm hyperactivated motility was also assessed. Sperm were capacitated in the presence of BAM15, NEN, or DMSO vehicle, and then their motility was measured by CASA. Interestingly, the DMSO vehicle, which did not impair basal motility or any other sperm parameters in our assays, interfered with human sperm hyperactivation at higher concentrations (IC_{50} of 0.004% DMSO) (Figure 3B), complicating interpretation of these results. However, NEN but not BAM15 significantly reduced curvilinear velocity beyond the deleterious effect of the DMSO vehicle (Supplementary Figure S3B). Raw data describing all measured sperm motility parameters are included as a supplemental dataset to this manuscript.

Small molecule uncouplers do not reduce human sperm ATP content or interfere with acrosome reaction

To investigate NEN and BAM15's mechanism of action on sperm motility (Figure 3, Supplementary Figure S3), their effects on sperm ATP concentrations were measured. Despite their impacts on the mitochondrial membrane potential, neither compound caused any change in ATP concentrations in non-capacitated (Figure 4A) or capacitated (Figure 4B) spermatozoa. Consistent with this finding, NEN and BAM15 had no effect beyond the DMSO vehicle on the ability of sperm to undergo either the spontaneous or ionophore-induced acrosome reaction (Supplementary Figure S4A, B). The acrosome reaction is a necessary pre-fertilization exocytotic event [28, 29] that exposes key fertilization receptors [30, 31]. In addition, pretreatment of mouse sperm with 10 μM NEN also did

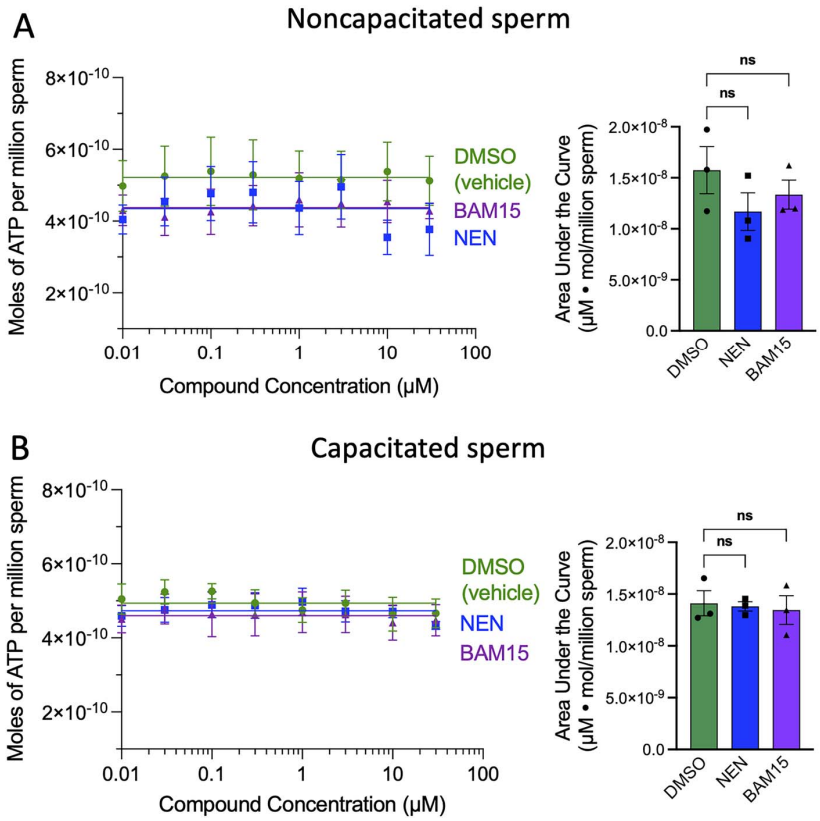

Figure 4. Effects of small molecule uncouplers on human sperm ATP production. (A) *Left*, quantification of ATP content of non-capacitated human sperm treated with compounds for 30 min. *Right*, AUC analysis of the plot to the left. (B) *Left*, quantification of ATP content of human sperm capacitated in the presence of compounds. *Right*, AUC analysis of the plot to the left. In both (A) and (B), AUC was calculated directly from data points, not from non-linear regression lines, and each data point represents the area under the curve for all concentrations of one biological replicate. Error bars in all plots represent SEM. Statistical significance in AUC analyses calculated using Dunnett's multiple comparisons test, and units in all AUC plots are the products of the *x* and *y* units in the relevant dose–response plot.

not impair in vitro fertilization between mouse sperm and eggs (Supplementary Figure S4C, D).

Discussion

In this study, we utilized a pair of small molecule uncouplers with different mechanisms of action to investigate the physiological roles of the mitochondrial membrane potential and plasma membrane potential in human sperm. Our data agree with data generated in other cell types [10, 11, 21] in finding that BAM15 specifically induces mitochondrial membrane uncoupling without causing uncoupling of the plasma membrane; in contrast, here we found that NEN leads to depolarization of both the mitochondrial and plasma membranes (Fig. 1). Given that there are no known uncoupling compounds that robustly depolarize the plasma membrane while leaving the mitochondrial membrane potential intact, this pairing of compounds is the best available way to tease apart the physiological importance of voltage across each of these membranes. The physiological effects of BAM15 are attributable specifically to the breakdown of mitochondrial membrane potential or its downstream effects, while any additive physiological effects of NEN over BAM15 are likely to be a result of the breakdown of the plasma membrane potential. This pairing of compounds could be a useful experimental system in a variety of cell types since it enables relatively quick interrogation of the relevance of these two membrane potentials to any measurable physiological property.

This study also investigated whether the gamete-specific ANT isoform ANT4 was expressed in the sperm plasma membrane, to rule out any possible ANT-mediation of NEN's plasma membrane effects. No immunocytochemical signaling was seen in the non-permeabilized plasma membrane (Supplementary Figure S2E), which suggests that ANT4 is likely not a transmembrane transporter of the sperm plasma membrane. In permeabilized sperm cells, once antibody concentration was titrated down to the lowest level that caused robust fluorescent signal, ANT4 signal became weak and intermittent in the principal piece of the flagellum but remained strong and consistent in the sperm midpiece. Although this is in contrast to one previous study [26], the mitochondrial localization observed here is consistent with the known localization of ANT1–3 and makes logical sense given ANT4's likely role as an ADP/ATP transmembrane transporter, based on its structural homology [32].

After confirming the mechanisms of action of these uncouplers, their effects on human sperm physiology and energy production were examined; both compounds had a dose-dependent inhibitory effect on sperm progressive

motility, with NEN having a more potent effect than BAM15 (Figure 3A). Next, the uncouplers' effects on hyperactivity were tested (Figure 3B), and although the DMSO vehicle had no negative effects in any other assays, it had a dose-dependent inhibitory effect on sperm hyperactivity which prevented meaningful interpretation of the effects of the uncouplers on hyperactivation. These results are corroborated by recent research showing that concentrations of DMSO vehicle below 0.5% have minimal effects on human sperm basal motility, vitality, and acrosome integrity, but may reduce tyrosine phosphorylation, a hallmark of capacitation [33]. Other investigators should be wary of this issue when designing future analyses of hyperactivation.

To investigate the root of the uncouplers' inhibition of basal motility, we analyzed their effect on ATP content in human sperm. There has been an ongoing debate in the field about whether oxidative phosphorylation or glycolysis is the primary source of ATP for human spermatozoa [34–36], with increasing evidence supporting the idea that glycolysis is sufficient to support many human sperm functions [18]. Our data support this conclusion, with both NEN and BAM15 failing to reduce human sperm's ATP content.

In addition to their role in ATP production, the mitochondria have also been suggested to regulate calcium homeostasis in the sperm [5]. Since the ability to sequester cations is dependent on a negative potential within the mitochondrial matrix, and the acrosome reaction is a calcium-evoked exocytotic event, we investigated whether NEN and BAM15 could affect sperm's ability to undergo the acrosome reaction. Interestingly, neither compound had a marked effect on either the rate of spontaneous acrosome reaction or calcium ionophore-induced acrosome reaction. Since the ability to undergo the acrosome reaction is dependent on successful capacitation, this result also suggests that the uncouplers did not impair that process even though sperm were exposed to them throughout the in vitro capacitation period.

The fact that NEN had a robust inhibitory effect on sperm basal motility while having no effect on ATP levels is likely due to its uncoupling of the sperm plasma membrane (Figure 1), which would affect many motility-related ion channels and intracellular signaling pathways that rely on a carefully moderated membrane potential for proper function [1]. Since BAM15 is known as a more mitochondria-specific uncoupler [10, 11, 21, 37] and did not induce plasma membrane current in the sperm electrophysiology assays (Figure 1), the mechanism of action of its more modest inhibition of basal progressive motility remains to be clarified.

Although this study found that ANT4 was indeed mitochondrially localized and that the ANT family of proteins can mediate NEN-induced uncoupling, the physiological data herein suggest that contraceptives that solely interfere with mature sperm oxidative phosphorylation will be unlikely to successfully inhibit key sperm functions. However, pairing an oxidative phosphorylation inhibitor with an inhibitor of a sperm-specific glycolytic enzyme, like lactate dehydrogenase C [38], might produce an effective contraceptive product. In addition, since niclosamide has been FDA approved for use in humans with a favorable safety profile [22], and possesses low bioavailability [39] and a pK_a near 6 [23] (close to the vaginal pH), it could be a useful ingredient in on-demand vaginal contraceptive products, where its deleterious effects on motility could make sperm less able to pass through the cervix and reproductive tract, and therefore less able to reach the egg.

Materials and methods

Ethic Statement

All experiments were performed in accordance with NIH guidelines for animal research and approved by UC Berkeley Animal Care and Use Committee (AUP 2015-07-7742), with every effort made to minimize animal suffering. All described methods are consistent with the recommendations of the Panel on Euthanasia of the American Veterinary Medical Association and IACUC committee. All experimental procedures utilizing human-derived samples were approved by the Committee on Human Research at the University of California, Berkeley, IRB protocol number 2013-06-5395.

Reagents

- Niclosamide ethanolamine was purchased from AdipoGen Life Sciences, #AG-CR1-3644.
- BAM15 was purchased from Sigma, product number SML1760-5MG.
- 2,4-Dinitrophenol was purchased from TCI, product D0109-25G.
- FCCP was purchased from Abcam, product code ab120081.
- MitoTracker Red CMX-Ros was purchased from ThermoFisher, #M7512.
- Polyclonal antibody to human ANT4—Novus Biologicals NBP1-89074 raised in rabbits against human ANT4 peptide.
- Mouse monoclonal antibody against human COX4l1—Proteintech #66110-1-Ig.
- Polyvinyl alcohol was purchased from Fluka, #81366-100G.
- A23187 was purchased from MilliporeSigma, #C7522-5MG.
- 10% goat serum from Invitrogen, #50-062Z.
- Bovine serum albumin from Sigma, #A3059-500G.

Sperm and reagent preparation

Human sperm cells were collected by masturbation from healthy donors and visually inspected for normal morphology and motility before use. Spermatozoa were isolated by the swim-up procedure in HTF solution (280 ± 5 mOsm, pH 7.3–7.4) or HS solution (320 ± 5 mOsm, pH 7.3–7.4) as previously described [40] and then concentrated by 5 min centrifugation at $\leq 500 \times g$ and supernatant removal. Swim-up was conducted in HTF solution except when conducting assays where significant concentrations of the swim-up supernatant would be mixed into subsequent incubations in HS solution, so as not to dilute the osmolarity to an intermediate level. The success of the swim-up protocol is identical in HTF and HS solution.

For all dose–response assays, NEN and BAM15 stocks were prepared at 10 mM in DMSO, then these stocks were added to the necessary aqueous media to each assay, such that 30 μM solutions contained 0.3% DMSO and 10 μM solutions contained 0.1% DMSO. These solutions were then serially diluted by 10× to lower concentrations, such that 1 μM solutions contained 0.01% DMSO, 100 nM solutions contained 0.001% DMSO, and so forth. All plots show DMSO on the same *x*-axis as compound concentration, to

indicate the amount of DMSO necessary to deliver that concentration of compound.

Flow cytometric assessment of MMP

Human sperm cells were incubated with small molecule uncouplers or vehicles in HS solution for 30 min at 37°C, then treated with 50 nM MitoTracker Red in the presence of either uncouplers or vehicles for an additional 30 min. Subsequently, cells were washed by centrifugation for 5 min at 500×*g*, supernatant was removed, and cells were resuspended in HS solution. Fluorescence was measured by flow cytometry on a BD LSR Fortessa Celeste or BD LSR Fortessa X20, using gates for size and density to exclude debris and aggregates, and a PE-Texas Red Filter set (561 nm laser excitation, 610/20 nm emission filter) to record fluorescence (Figure 1, Supplementary Figure S1). Fluorescence midpiece location was confirmed by microphotography on an Olympus IX71 inverted microscope using a Hamamatsu Orca-ER digital camera and a 60× Olympus UPlanSApo objective (Figure 1). Fluorescence statistics were analyzed using Microsoft Excel version 16 and GraphPad Prism version 9. The subpopulation of cells with the highest Gaussian distribution of fluorescence were manually gated and the mean fluorescence of this population was normalized to the average of the means of the same population in the relevant vehicle control samples of each run. Each data point represents the mean fluorescence of the highest normally distributed peak in an individual flow cytometry run of 10 000 cells. Non-linear least-squares regression was performed using an unweighted [inhibitor] versus response three-parameter model (Hill slope = −1.0), identifying "unstable" fits. Outliers were tested using a ROUT coefficient of 1%, with no outliers detected. Residuals were checked for normality using the D'Agostino–Pearson omnibus normality test, checked for clustering using the Replicates test, and checked for appropriate weighting using the homoscedasticity test.

Area-under-the-curve analysis

For all dose–response plots, area under the curve (AUC) analysis was performed using the trapezoid method ($\Delta X^* (Y_1 + Y_2)/2$) on the arithmetic means of the measured parameter at each compound concentration. Each data point represents the AUC of all concentrations tested in one biological replicate. Effects of each compound were then compared using Dunnett's multiple comparisons test.

Sperm motility assessment

Isolated human sperm were incubated with small molecule uncouplers and vehicles at 37°C for 30 min, after which they were mixed with 1% polyvinyl alcohol to prevent adherence to glass and loaded into a Leja Standard Count 2-chamber sperm analysis slide (depth 20 μm). Sperm motility was analyzed on a Hamilton-Thorne IVOS I computer-aided sperm analyzer, at 37°C. Motility was measured for least 500 cells in each condition. Progressive motility was defined using Hamilton-Thorne's proprietary software module. Non-linear least-squares regression was performed by GraphPad Prism version 9 using an unweighted [inhibitor] versus response three-parameter model (Hill slope = −1.0), identifying "unstable" fits. Outliers were tested using a ROUT coefficient of 1% and none were identified. Residuals were checked for normality using the D'Agostino–Pearson omnibus normality test, checked for clustering using the Replicates test, and checked for appropriate weighting using the homoscedasticity test. Residuals for NEN and BAM15 passed all tests, except that BAM15 failed the test for homoscedasticity with a *P* value of 0.0207.

To study the effect of uncouplers on human sperm hyperactivated motility, cells were incubated for ≥3 h in capacitation media (20% fetal bovine serum (FBS) and 25 mM sodium bicarbonate in HS solution) at 37°C and 5% CO_2 in the presence of various concentrations of uncouplers or DMSO vehicle. Motility was then measured on a Hamilton–Thorne IVOS II computer-aided sperm analyzer as above (except without the addition of polyvinyl alcohol), with the definition for hyperactivated motility set as VCL >150 μm/s AND LIN <50% AND ALH >7.0 μm [41, 42].

Flow cytometric assessment of acrosome status

Human sperm cells were incubated for 3.5 h in capacitation media (20% FBS and 25 mM sodium bicarbonate in HS solution) at 37°C and 5% CO_2. In the final hour of incubation, custom monoclonal antibodies raised in mouse hybridoma cells against the ectodomain of human Izumo1 were added, at a concentration of 10 μg/mL. Subsequently, 50 μM A23187 was added, and cells were incubated at 37°C and 5% CO_2 for an additional 30 min, after which cells were washed by centrifugation 3× (500×*g*, 5 min) in HS solution, incubated 30 min at room temperature with a goat anti-mouse 647 secondary antibody (Invitrogen A32728, final concentration 4 μg/mL) in 10% goat serum. After an additional three washes by centrifugation, propidium iodide (PI) was added to a final concentration of 1 μg/mL, and cells were analyzed by flow cytometry using the same instrumentation as above, except that Izumo-647 was visualized using an APC filter set (bandpass 670/30 or 670/14 nm) and PI was visualized using a PE-Texas Red filter set (bandpass 610/20 nm). Izumo-647-positive cells were scored as acrosome reacted since the Izumo protein is known to be expressed only inside the acrosome, which in living non-permeabilized cells becomes accessible to external antibodies only after the acrosome reaction. PI-negative cells were scored as living.

Generation of IZUMO1 monoclonal antibody using mouse hybridoma

The IZUMO1 monoclonal antibodies were generated from mouse hybridoma and characterized as previously described [43]. Briefly, IZUMO1 antibodies 4E04 and 6F02 belong to the murine IgG1 isotype with kappa light chain. For antibody production, hIZUMO1-positive hybridomas were cultured in medium containing 10% FBS and subsequently adapted to an FBS-free medium. The condition media were harvested, and the IgG antibodies were purified by protein G affinity chromatography and by Superdex-200 gel filtration chromatography in a buffer of 150 mM NaCl, 20 mM HEPES pH 7.4. Purified IgG antibodies were concentrated to 1 mg/mL with the addition of 10% (v/v) glycerol for use.

ATP assessment

Human sperm cells were incubated with uncoupler compounds or vehicle for 1 h at 37°C in white 96-well Costar polystyrene assay plates, under sterile conditions. ATP content was assessed using a PerkinElmer ATPlite Luminescence Assay System Kit, according to manufacturer instructions, and luminescence was imaged on a Biotek Synergy H4 Hybrid

plate reader, set to endpoint/kinetic setting (one measurement point per well), with 1 s of integration time and a manual gain setting of 135. ATP content was quantified by averaging three technical replicates, then interpolating against a standard curve of ATP solutions, per manufacturer instructions. Nonlinear least-squares regression was performed by GraphPad Prism version 9 using an [inhibitor] versus response three-parameter model (Hill slope = −1.0), weighted by $1/Y^2$, identifying "ambiguous" fits. Outliers were tested using a ROUT coefficient of 1%, with no outliers detected. Residuals were checked for normality using the D'Agostino–Pearson omnibus normality test, checked for clustering using the Replicates test, and checked for appropriate weighting using the homoscedasticity test, and passed all tests.

Mouse in vitro fertilization

All mice were kept in the Animal Facility of the University of California, Berkeley, fed standard chow diet (PicoLab Rodent diet 20, #5053; LabDiet), and hyper-chlorinated water ad libitum in a room with controlled light (14 h light, 10 h darkness) and temperature (23 ± 0.5°C). Animals were humanely killed by CO_2 asphyxiation and cervical dislocation according to ACUC guidelines with every effort made to minimize suffering.

C57Bl/6N (Charles River) female mice between 4 and 16 weeks old were superovulated by intraperitoneal injection of 5 IU pregnant mare serum gonadotropin (Sigma, G4877) and 48 h later, 5 IU human chorionic gonadotropin (hCG; Millipore, 230734). Thirteen hours after hCG injection, the females were euthanized and cumulus–oocyte complexes were collected from the oviduct ampulla in HTF medium (Embryomax, Specialty Media; Millipore) and incubated for 30 min at 37°C and 5% CO_2 prior to insemination. Simultaneously, mouse sperm were isolated from the cauda epididymis as previously described[36] and allowed to capacitate at 37°C and 5% CO_2 for 60–90 min using commercial HTF medium for mouse in vitro fertilization (IVF) (Embryomax, Specialty Media; Millipore) in the presence of uncoupler compounds or control vehicle. Sperm and eggs were then mixed to a final concentration of 210 000 sperm/mL in 600 μL of HTF medium and incubated at 37°C and 5% CO_2 for 4 h. Afterwards, the eggs were washed by mouth pipetting in HTF media to remove excess sperm. A final wash in KSOM media (Zenith Biotech) supplemented with 1 mg/mL bovine serum albumin (BSA) was then done before dividing the eggs into 10 μL drops of KSOM/BSA media overlaid with embryo-tested light mineral oil (Millipore) for culture at 37°C, 5% CO_2. Best efforts were made to divide equal numbers of eggs from each mouse into control and uncoupler-treated conditions. Then, 3.5 days following IVF, the number of fertilized eggs was determined visually by assessing the percentage of embryos that reached morula or blastula stage.

Sperm whole-cell electrophysiology

Whole-cell electrophysiology was performed on isolated human sperm cells as described previously [44, 45]. Once sperm cell "break in" was achieved in HS solution, cells were subjected to a voltage ramp protocol in the presence of bath and pipette solutions designed to ensure that only H^+ current across the membrane was measured. Intracellular (pipette) solution contained 150 mM NMDG, 5 mM BAPTA, 100 mM HEPES, and 1 mM Tris chloride, pH 7.5 with $MeSO_3$. Extracellular (bath) solution contained 157 mM NMDG, 20 mM MES, 1 mM $MgCl_2$, 100 μM $ZnCl_2$, pH 6, with $MeSO_3$. Compounds and vehicles were applied by perfusion, and currents were recorded until they showed a minimal change between subsequent voltage ramps. Then, compounds were washed out and subsequent compounds added once currents had returned to baseline values. Representative traces and time courses were created in Origin Pro version 9.0.0 and statistical analysis performed in GraphPad Prism 9.

Mitochondrial patch-clamp electrophysiology

Mouse heart mitochondria were isolated from wildtype and $ANT1^{-/-}$ C57BL/6J2z mice and mitoplasts prepared and patch-clamped as described previously [24]. Both the bath and pipette solutions were formulated to record H^+ currents and contained only salts that dissociate into large anions and cations that are normally impermeant through ion channels or transporters. Pipettes were filled with 130 mM tetramethylammonium hydroxide (TMA), 1.5 mM EGTA, 2 mM Tris chloride, and 100 mM HEPES (or MES). pH was adjusted to 7.5 with D-gluconic acid, and tonicity was adjusted to ∼360 mmol/kg with sucrose. Bath solution contained 100 mM HEPES (or MES) and 1 mM EGTA (pH adjusted to 7.0 with Trizma base, and tonicity adjusted to ∼300 mmol/kg with sucrose).

Immunocytochemistry

Briefly, sperm were adhered onto poly-D-lysine-coated coverslips and, in some experiments, incubated 15 min at 37°C with 50 nM MitoTracker Red CMXRos, then washed and fixed in 4% PFA for 10 min, and washed and additionally fixed in ice-cold methanol for 1 min. Cells were permeabilized and blocked in 5% BSA and 0.1% Triton X-100 in PBS for 45 min, then incubated overnight at 4°C with rabbit polyclonal antibody against human ANT4 (Novus #NBP1-89074, used at 0.08 μg/mL) and, in some experiments, a mouse monoclonal antibody against COXIV (COX4l1) (Proteintech #66110-1-Ig, used at 6.8 μg/mL). After washing, samples were incubated with secondary antibodies (Jackson Alexa Fluor 647 AffiniPure Donkey Anti-Rabbit IgG (H + L) (code 711-605-152) at a dilution of 1:1000, and Jackson ImmunoResearch anti-mouse Cy3 or Molecular Probes A10521 goat anti-mouse Cy3 at a dilution of 1:1000) for 45 min, then washed and mounted using ProLong Gold Antifade mountant with DAPI.

Cells were imaged on an Olympus FV3000 inverted laser scanning confocal microscope, using an Olympus UPLSAPO Super Apochromat 60× oil immersion objective (NA 1.35) and Olympus Z-81226 immersion oil. Laser scanning was performed by galvanometer, unidirectionally at a rate of 2 μs/pixel with no averaging, with pixel sizes of 0.207 μm/pixel in the *x* and *y* directions. Multiple colors were imaged in line-by-line sequential scanning mode, and multiple *z*-planes were acquired with a thickness of 0.47 μm, on a linear-encoded stage. Images displayed are maximum intensity *z*-stacks of all relevant *z*-planes. All colors were imaged with a pinhole diameter of 233 μM, and laser illumination was passed through a 10% neutral density filter. DAPI was illuminated by a 405 nm laser set to 3% power, and emitted light was passed through a 430–470 nm emission filter and detected with a photomultiplier tube (PMT) set to 500 V. Cy3 was illuminated by a 561 nm laser set to 4% power, with a 570–620 nm emission filter and a PMT set to 500 V. Alexa 674 was illuminated by a 642 nm laser set to 4%

power, with a 650–750 nm emission filter and a PMT set to 550 V.

Super-resolution microscopy

ICC slides made as described above were imaged using three-dimensional stochastic optical reconstruction microscopy (3D-STORM) [46, 47] performed on a home-built setup using a Nikon CFI Plan Apo λ 100× oil immersion objective (NA 1.45), as described previously [48]. In brief, the sample was mounted with an imaging buffer consisting of 5% (w/v) glucose, 100 mM cysteamine, 0.8 mg ml^{-1} glucose oxidase and 40 μg ml^{-1} catalase in a Tris–HCl buffer (pH 7.5). For two-color imaging of COXIV and ANT4, the two targets were labeled by Alexa Fluor 647 and CF568, respectively, and were imaged sequentially using 647 and 560 nm excitation lasers. These lasers were passed through an acousto-optic tunable filter and illuminated a few micrometers into the sample at around 2 kW cm^{-2}, thus photoswitching most of the labeled dye molecules in the sample into the dark state while allowing a small, random fraction of molecules to emit across the wide-field over different camera frames. Single-molecule emission was passed through a cylindrical lens of focal length 1 m to introduce astigmatism [47], and recorded with an Andor iXon Ultra 897 EM-CCD camera at a frame rate of 110 Hz, for a total of around 50 000 frames per image. Data acquisition used publicly available software (https://github.com/ZhuangLab/storm-control). The raw STORM data were analyzed using Insight3 software [47] according to previously described methods [46, 47]. Secondary antibodies used Alexa Fluor 647-labeled goat anti-mouse (Invitrogen, A21236, 1:400) and donkey anti-rabbit (Jackson ImmunoResearch, 711-005-152, 1:70) conjugated with CF568 succinimidyl ester (Biotium, 92131).

Western blotting

Human sperm or HEK293 cells were lysed by addition of $RIPA^{++}$ buffer (composition: 50 mM Tris HCl, pH 7.4; 150 mM NaCl; 1% Triton X-100; 0.5% sodium deoxylcholate; 0.1% sodium dodecyl sulfate; 1 mM EDTA; 10% glycerol; with Pierce Protease inhibitor tablet or solution added to manufacturer's instructions), then homogenized by 25 passes through a 21-gauge or smaller syringe, then shook on ice for 30 min, and centrifuged at 12 000 rpm at 4°C for 20 min, after which the supernatant was collected and frozen at −80°C. After thawing, protein concentration was assessed using a Pierce Rapid Gold BCA Protein Assay Kit, per manufacturer instructions, and measured on a Biotek Synergy H4 Hybrid plate reader. A target of 30 μg of protein was mixed with 4× Laemmli buffer and beta-mercaptoethanol, heated for 10 min at 99°C, then loaded to each well of a precast 4–20% mini-Protean TGX gel (Bio-Rad), and run in an electrophoresis chamber until ladder bands were well resolved. Transfer onto a PVDF membrane was accomplished with an Invitrogen iBlot Dry Blotting System, following manufacturer instructions, at 20 V for 7 min. After washing 3× with PBS with 0.1% Tween (PBST), the membrane was blocked in 3% BSA for 15–30 min, then incubated rocking with primary antibody overnight at 4°C. The following day, the membrane was washed 3× with PBST and incubated with a 1:15 000 dilution of HRP-conjugated Abcam Ab6721 Goat pAb anti-Rabbit IgG secondary antibody for 1 h at room temperature. After 3× PBST washes and 2× PBS washes, bands were visualized using a Prometheus ProSignal Pico kit, per instructions, and imaged in a ProteinSimple FluorChem M. Afterwards, images were inverted, rotated, and cropped in ImageJ 1.52a.

Supplementary data

Supplementary data are available at *BIOLRE* online.

Conflict of interest

WMS, PVL, ET, AMB, and YK are co-inventors on a patent related to this work, which UC Berkeley has licensed to YourChoice Therapeutics, for which PVL is a co-founder and YK is a shareholder. The other authors declare no competing interests.

Data availability

All data used to support the conclusions in this study appear in the main and supplementary figures.

Author contributions

WMS and PVL conceived the project and designed experiments. WMS conducted most experiments and analyzed most data, except as noted below, and wrote the manuscript. NTP and WMS performed in vitro fertilization experiments. BU and WMS conducted STORM and BU analyzed data, under supervision of KX. S.T. produced Izumo1 antibodies used during acrosome reaction assays. ET and JL assisted with multiple experiments. LJ and JS enabled access to and training on computer-aided sperm analysis machines for motility assays performed by WMS. AMB performed mitochondrial patch-clamp experiments and analyzed that data, under supervision of YK and PVL. And WMS performed human sperm patch-clamp electrophysiology. All of the authors discussed the results and commented on the manuscript.

Conceptualization: WMS and PVL
Data curation: WMS
Formal analysis: WMS and AMB
Funding acquisition: PVL and WMS
Investigation: WMS, NTP, BU, ET, JL, AMB, and PVL
Methodology: WMS, BU, AMB, and PVL
Project administration: WMS
Resources: WMS, ST, LJ, JS, KX, YK, and PVL
Supervision: JS, KX, YK, and PVL
Validation: WMS
Visualization: WMS, BU, and AMB
Writing—original draft preparation: WMS
Writing—review & editing: all authors

References

1. Vyklicka L, Lishko PV. Dissecting the signaling pathways involved in the function of sperm flagellum. *Curr Opin Cell Biol* 2020; **63**: 154–161.
2. Molina LCP, Gunderson S, Riley J, Lybaert P, Borrego-Alvarez A, Jungheim ES, Santi CM. Membrane potential determined by flow cytometry predicts fertilizing ability of human sperm. *Front Cell Dev Biol* 2020; **7**:387.
3. Brown SG, Publicover SJ, Mansell SA, Lishko PV, Williams HL, Ramalingam M, Wilson SM, Barratt CLR, Sutton KA, Da Silva SM. Depolarization of sperm membrane potential is a common feature of men with subfertility and is associated with low fertilization rate at IVF. *Hum Reprod* 2016; **31**:1147–1157.
4. Irigoyen P, Pintos-Polasky P, Rosa-Villagran L, Skowronek MF, Cassina A, Sapiro R. Mitochondrial metabolism determines the functional status of human sperm and correlates with semen parameters. *Front Cell Dev Biol* 2022; **10**:926684.

5. Boguenet M, Bouet P-E, Spiers A, Reynier P, May-Panloup P. Mitochondria: their role in spermatozoa and in male infertility. *Hum Reprod Update* 2021; **27**:697–719.
6. Zhang G, Wang Z, Ling X, Zou P, Yang H, Chen Q, Zhou N, Sun L, Gao J, Zhou Z, Cao J, Ao L. Mitochondrial biomarkers reflect semen quality: results from the MARCHS study in Chongqing, China. *PLOS One* 2016; **11**:e0168823.
7. Zhang G, Yang W, Zou P, Jiang F, Zeng Y, Chen Q, Sun L, Yang H, Zhou N, Wang X, Liu J, Cao J et al. Mitochondrial functionality modifies human sperm acrosin activity, acrosome reaction capability and chromatin integrity. *Hum Reprod* 2019; **34**:3–11.
8. Childress ES, Alexopoulos SJ, Hoehn KL, Santos WL. Small molecule mitochondrial uncouplers and their therapeutic potential. *J Med Chem* 2018; **61**:4641–4655.
9. Bielawski J, Thompson TE, Lehninger AL. The effect of 2,4-dinitrophenol on the electrical resistance of phospholipid bilayer membranes. *Biochem Biophys Res Commun* 1966; **24**:948–954.
10. Kenwood BM, Weaver JL, Bajwa A, Poon IK, Byrne FL, Murrow BA, Calderone JA, Huang L, Divakaruni AS, Tomsig JL, Okabe K, Lo RH et al. Identification of a novel mitochondrial uncoupler that does not depolarize the plasma membrane. *Mol Metab* 2014; **3**:114–123.
11. Bertholet AM, Natale AM, Bisignano P, Suzuki J, Fedorenko A, Hamilton J, Brustovetsky T, Kazak L, Garrity R, Chouchani ET, Brustovetsky N, Grabe M et al. Mitochondrial uncouplers induce proton leak by activating AAC and UCP1. *Nature* 2022; **606**: 180–187.
12. Dolce V, Scarcia P, Iacopetta D, Palmieri F. A fourth ADP/ATP carrier isoform in man: identification, bacterial expression, functional characterization and tissue distribution. *FEBS Lett* 2005; **579**:633–637.
13. Lim CH, Brower JV, Resnick JL, Oh SP, Terada N. Adenine nucleotide translocase 4 is expressed within embryonic ovaries and dispensable during oogenesis. *Reprod Sci* 2015; **22**:250–257.
14. Brower JV, Rodic N, Seki T, Jorgensen M, Fliess N, Yachnis AT, McCarrey JR, Oh SP, Terada N. Evolutionarily conserved mammalian adenine nucleotide translocase 4 is essential for spermatogenesis. *J Biol Chem* 2007; **282**:29658–29666.
15. Hamazaki T, Leung W-Y, Cain BD, Ostrov DA, Thorsness PE, Terada N. Functional expression of human adenine nucleotide translocase 4 in *Saccharomyces cerevisiae*. *PloS One* 2011; **6**:e19250.
16. Leung W-Y, Hamazaki T, Ostrov DA, Terada N. Identification of adenine nucleotide translocase 4 inhibitors by molecular docking. *J Mol Graph Model* 2013; **45**:173–179.
17. Zhang Y, Tian D, Matsuyama H, Hamazaki T, Shiratsuchi T, Terada N, Hook DJ, Walters MA, Georg GI, Hawkinson JE. Human adenine nucleotide translocase (ANT) modulators identified by high-throughput screening of transgenic yeast. *J Biomol Screen* 2016; **21**:381–390.
18. Hereng TH, Elgstøen KBP, Cederkvist FH, Eide L, Jahnsen T, Skålhegg BS, Rosendal KR. Exogenous pyruvate accelerates glycolysis and promotes capacitation in human spermatozoa. *Hum Reprod* 2011; **26**:3249–3263.
19. Gallon F, Marchetti C, Jouy N, Marchetti P. The functionality of mitochondria differentiates human spermatozoa with high and low fertilizing capability. *Fertil Steril* 2006; **86**:1526–1530.
20. Paoli D, Gallo M, Rizzo F, Baldi E, Francavilla S, Lenzi A, Lombardo F, Gandini L. Mitochondrial membrane potential profile and its correlation with increasing sperm motility. *Fertil Steril* 2011; **95**: 2315–2319.
21. Firsov AM, Popova LB, Khailova LS, Nazarov PA, Kotova EA, Antonenko YN. Protonophoric action of BAM15 on planar bilayers, liposomes, mitochondria, bacteria and neurons. *Bioelectrochemistry* 2021; **137**:107673.
22. Kadri H, Lambourne OA, Mehellou Y. Niclosamide, a drug with many (re)purposes. *ChemMedChem* 2018; **13**:1088–1091.
23. Jurgeit A, McDowell R, Moese S, Meldrum E, Schwendener R, Greber UF. Niclosamide is a proton carrier and targets acidic endosomes with broad antiviral effects. *PLoS Pathog* 2012; **8**:e1002976.
24. Bertholet AM, Chouchani ET, Kazak L, Angelin A, Fedorenko A, Long JZ, Vidoni S, Garrity R, Cho J, Terada N, Wallace DC, Spiegelman BM et al. H + transport is an integral function of the mitochondrial ADP/ATP carrier. *Nature* 2019; **571**:515.
25. Levy SE, Chen Y-S, Graham BH, Wallace DC. Expression and sequence analysis of the mouse adenine nucleotide translocase 1 and 2 genes. *Gene* 2000; **254**:57–66.
26. Kim Y-H, Haidl G, Schaefer M, Egner U, Mandal A, Herr JC. Compartmentalization of a unique ADP/ATP carrier protein SFEC (sperm flagellar energy carrier, AAC4) with glycolytic enzymes in the fibrous sheath of the human sperm flagellar principal piece. *Dev Biol* 2007; **302**:463–476.
27. World Health Organization. *WHO Laboratory Manual for the Examination and Processing of Human Semen*, 6th ed. Geneva: World Health Organization; 2021.
28. Brucker C, Lipford GB. The human sperm acrosome reaction: physiology and regulatory mechanisms. An update. *Hum Reprod Update* 1995; **1**:51–62.
29. Hirohashi N, Yanagimachi R. Sperm acrosome reaction: its site and role in fertilization. *Biol Reprod* 2018; **99**:127–133.
30. Satouh Y, Inoue N, Ikawa M, Okabe M. Visualization of the moment of mouse sperm–egg fusion and dynamic localization of IZUMO1. *J Cell Sci* 2012; **125**:4985–4990.
31. Balestrini PA, Jabloñski M, Schiavi-Ehrenhaus LJ, Marín-Briggiler CI, Sánchez-Cárdenas C, Darszon A, Krapf D, Buffone MG. Seeing is believing: current methods to observe sperm acrosomal exocytosis in real time. *Mol Reprod Dev* 2020; **87**: 1188–1198.
32. Palmieri F, Monné M. Discoveries, metabolic roles and diseases of mitochondrial carriers: a review. *Biochim Biophys Acta BBA - Mol Cell Res* 2016; **1863**:2362–2378.
33. Bisconti M, Grosjean P, Arcolia V, Simon J-F, Hennebert E. Influence of two widely used solvents, ethanol and dimethyl sulfoxide, on human sperm parameters. *Int J Mol Sci* 2023; **24**: 505.
34. du Plessis SS, Agarwal A, Mohanty G, van der Linde M. Oxidative phosphorylation versus glycolysis: what fuel do spermatozoa use? *Asian J Androl* 2015; **17**:230–235.
35. Ford WCL. Glycolysis and sperm motility: does a spoonful of sugar help the flagellum go round? *Hum Reprod Update* 2006; **12**:269–274.
36. Storey BT. Mammalian sperm metabolism: oxygen and sugar, friend and foe. *Int J Dev Biol* 2008; **52**:427–437.
37. Kenwood BM, Calderone JA, Taddeo EP, Hoehn KL, Santos WL. Structure–activity relationships of furazano[3,4-b]pyrazines as mitochondrial uncouplers. *Bioorg Med Chem Lett* 2015; **25**: 4858–4861.
38. Goldberg E. The sperm specific form of lactate dehydrogenase (LDHC4) is required for fertility and is an attractive target for male contraception (a review). *Biol Reprod* 2021; **104**:521–526.
39. Zhang X, Zhang Y, Zhang T, Zhang J, Wu B. Significantly enhanced bioavailability of niclosamide through submicron lipid emulsions with or without PEG-lipid: a comparative study. *J Microencapsul* 2015; **32**:496–502.
40. Skinner WM, Mannowetz N, Lishko PV, Roan NR. Single-cell motility analysis of tethered human spermatozoa. *Bio-Protoc* 2019; **9**:e3182.
41. Mortimer ST, van der Horst G, Mortimer D. The future of computer-aided sperm analysis. *Asian J Androl* 2015; **17**:545–553.
42. Mortimer D, Mortimer ST. Routine application of CASA in human clinical andrology and ART laboratories. In: Björndahl L, Flanagan J, Holmberg R, Kvist U (eds.), *XIIIth International Symposium on Spermatology*. Cham: Springer International Publishing; 2021: 183–197.

43. Tang S, Lu Y, Skinner WM, Sanyal M, Lishko PV, Ikawa M, Kim PS. Human sperm TMEM95 binds eggs and facilitates membrane fusion. *Proc Natl Acad Sci USA* 2022; **119**:e2207805119.
44. Liu B, Mundt N, Miller M, Clapham DE, Kirichok Y, Lishko PV. Recording electrical currents across the plasma membrane of mammalian sperm cells. *JoVE J Vis Exp* 2021; **168**:e62049.
45. Kirichok Y, Lishko PV. Rediscovering sperm ion channels with the patch-clamp technique. *MHR Basic Sci Reprod Med* 2011; **17**: 478–499.
46. Rust MJ, Bates M, Zhuang X. Sub-diffraction-limit imaging by stochastic optical reconstruction microscopy (STORM). *Nat Methods* 2006; **3**:793–796.
47. Huang B, Wang W, Bates M, Zhuang X. Three-dimensional super-resolution imaging by stochastic optical reconstruction microscopy. *Science* 2008; **319**:810–813.
48. Wojcik M, Hauser M, Li W, Moon S, Xu K. Graphene-enabled electron microscopy and correlated super-resolution microscopy of wet cells. *Nat Commun* 2015; **6**:7384.